Scientific Journal of Astana IT University
ISSN (P): 2707-9031 ISSN (E): 2707-904X
VOLUME 15, SEPTEMBER 2023

DOI: 10.37943/15AHSE8085

Balgaisha Mukanova
Doctor of Mathematical and Physical Sciences, Full Professor of the Department Computations and Data Science
balgaisha.mukanova@astanait.edu.kz, orcid.org/0000-0002-0823-6451
Astana IT University, Kazakhstan

SIMPLIFIED ADAPTIVE TRIANGULATION OF THE CONTACT BOUNDARIES OF THE DAM MODEL

Abstract: To numerically solve the system of integral equations, it is customary to establish a discrete grid within each integration area. In the context of 3D modeling, these areas correspond to surfaces situated in space. The standard discretization technique employed for the computational domain is triangulation. This study addresses the integral equation system pertinent to the electrical tomography of dams. The structural model encompasses an embankment dam, the upstream and downstream water bodies, the dam's base, and a potential leakage region on the upstream side. An alternative configuration may be encountered in specific scenarios with no water downstream. Consequently, the model may incorporate up to nine distinct contact boundaries. Accordingly, the system of integral equations comprises an equivalent number of equations. Effectively resolving this system through numerical methods necessitates applying triangulation techniques to these diverse surfaces. While mathematical packages like Matlab offer triangulation functions, they may not fully address the specific demands of the problem. Additionally, the grid resolution should be heightened in proximity to key elements such as the sounding line, the supply electrode, and the various contact lines within the medium. These considerations transform the triangulation task into a distinct subtask within the numerical simulation of the resistivity tomography problem. In this paper, we provide our specific approach to this problem. The simplification of the triangulation algorithm is rooted in the predominant utilization of the two-dimensional geometric properties inherent to the object under study. For most contact boundaries, the triangulation is constructed layer by layer with a gradual modulation in triangle dimensions as one progresses from one layer to the next, orthogonal to the axis of the dam. Concerning the surface corresponding to the leakage area, cylindrical coordinates are used for surface parameterization. This approach enables partitioning the surface into discrete strata, facilitating a systematic, layer-by-layer grid construction. Additionally, points at the intersections of contact boundaries are integrated into the pre-existing triangulation by applying a standard function within the Matlab package. In the future, the mathematical modeling based on the Integral Equation Method with adaptive discretization will help incorporate real-time computations into information systems related to monitoring hydraulic structures.

Keywords: ERT; dam sounding; integral equations; triangulation; adaptive grid.

Introduction

Modern IT development creates opportunities to develop Geographic Information Systems (GIS) for monitoring hydraulic structures by integrating field measurement data into a database. One of the primary methods employed for surveying dams and similar structures today is

Received: 15.08.2023 Accepted: 17.09.2023 Published: 30.09.2023

DOI: 10.37943/15AHSE8085

Electrical Resistivity Tomography (ERT). This method has been extensively researched by Barker (1981, 1992, [1],[2]), Dahlin (1993, 1996, 2001, 2007, [3-6]), Gunter and Rucker (2003, [7]), and others. The data obtained through ERT are processed using interpretation software. These programs are built upon equations describing a static electric field in a non-uniform medium and utilize methods for solving inverse problems (Loke and Barker, 1996, [8]; Loke, 2000, [9]). However, interpreting this data presents a complicated task that demands powerful computers and specialized software, posing challenges for real-time integration with GIS.

Conversely, addressing the direct mathematical modeling problems is more cost-effective, enabling us to consider complementing information systems with a mathematical modeling component. In this scenario, achieving real-time simulation results becomes a desirable goal. From this perspective, efficient and high-precision calculation methods, such as the method of integral equations, are of great importance. However, implementing this method necessitates the development of fast algorithms for discretizing the computational domain which constitutes the focal point of this study.

As mentioned above, mathematical modeling plays an important role in result interpretation. It proves especially valuable when dealing with complex sounding conditions caused by surface topography or material inclusions. Through modeling, we can visualize and quantitatively assess the impact of these conditions on measurement outcomes. For instance, in the article (Turarova et al., 2022, [10]), explicit computations elucidate the influence of the three-dimensional medium structure on 2D inversion results. The papers (Rakisheva, Mukanova, 2021, [11]) and (Rakisheva et al., 2021, [12]) show numerically how relief features affect sounding curves. In the monograph (Mukanova, Modin, 2018, [13]), various examples of ERT method simulations are presented via the formulation of integral equations. The article (Turarova et al., 2022, [14]) is dedicated to explicitly calculating sounding curves in the presence of surface relief and developing a method to filter out nonphysical anomalies from interpretation results. Generally speaking, articles [10] and [11] emphasize the advantages of the integral equation method compared to techniques that necessitate the discretization of the entire three-dimensional domain, a common approach in the mathematical modeling of 3D problems. Applications of the finite element method and integral equations to problems in electrodynamics are also discussed in the monographs [14] (Shi-zhe Xu, 2001) and [15] (Zhdanov, 2015). The first of these monographs focuses on two-dimensional formulations, while the second formulates integral equations for three-dimensional problems in which unknown functions are defined on 2D surfaces.

When comparing our approach to the methods outlined by [14] and [15], we reduce the problem to the Fredholm equation of the second kind. Another difference is that we formulate the problem involving infinite areas and consider the medium's boundary with air. Additionally, a practical case of the ERT method of dam probing is considered.

It is important to note that applying the integral equation method has limitations. Specifically, this method is most effective when dealing with geological or geoelectric environments characterized by well-defined boundaries. Such characteristics are commonly found in artificially constructed settings, such as dams and embankments. An additional requirement for the method's applicability involves discretizing all emerging contact surfaces. In scenarios characterized by predominantly two-dimensional geometry, it becomes possible to reduce the problem by applying Fourier transformations. This transformation reduces the problem into a series of one-dimensional equations, thereby simplifying the discretization process to grid points distributed along curve segments (Rakisheva, Mukanova, 2021, [11]).

In contrast, in the 3D case, the discretization is performed on the contact surfaces, delineating different media regions for three-dimensional structures. To reduce computational costs,

Scientific Journal of Astana IT University
ISSN (P): 2707-9031 ISSN (E): 2707-904X
VOLUME 15, SEPTEMBER 2023

one needs to reduce the dimensionality of the grid. For 3D problems, discretizing even relatively simple environment models can yield grids comprising tens of thousands of elements (Turarova et al., [16]).

The numerical solution of integral equations entails computationally intensive processes involving dense matrices whose dimensions are proportional to the square of the number of grid nodes. Consequently, solving such tasks in real-time on most personal computers proves challenging due to the memory limitations of the computing devices.

Nevertheless, the computational benefits that arise from employing grids tailored to the specific problem at hand are well recognized Frey and George, 2008, [17]).

The earliest applications of triangulation-based computational grids are associated with implementing the finite element method in solid mechanics, fluid dynamics, and other problems formulated in terms of partial differential equations. In the case of geometrically complex objects, the triangulation problem is recognized as a distinct area of research. For instance, in (Cuillière, 1998, [18]), an algorithm is introduced for the automatic adaptive triangulation of parametrically defined surfaces with intricate shapes, along with a priori mesh density estimation. The article [19] (Lo, 2002) provides an overview of the application of the finite element method and triangulation in continuum mechanics and engineering problems, discussing prospects for further applications.

Currently, the focus of triangulation problems is shifting towards constructing surfaces for three-dimensional objects in computer graphics and industry (Feng et al., 2018, [20]; Schmidt et al., 2023, [21]).

Geodesy and cartography problems also employ triangulation to depict terrain, and they possess distinctive characteristics related to the requirement for conformity with the object's boundaries and the environmental surface. For instance, in [21] (Schmidt et al., 2023), authors address the challenge of presenting two triangulations while enabling the assessment of distortions and the acceleration of the triangulation conversion algorithm when altering map resolutions.

Research on algorithms for constructing triangulations, which necessitates considering the geometric features of the discretization area and the specifics of the problem formulation, is also ongoing. For instance, the works [22] (Shewchuk, 2000) and [23] (Meng and Mei, 2013) are dedicated to the construction of triangulations for complex regions characterized by boundaries containing acute angles, while the work [24] by Schier and Klein (2023) explores the conditions for constructing a triangulation that guarantees the precise satisfaction of the integral dependencies arising from the formulation of the partial differential problem.

The lecture notes [25] by Shewchuk (2012) examine the most applied algorithms for constructing Delaunay triangulation and propose a classification. The complexity of each algorithm was assessed under both favorable and unfavorable conditions. It is shown that the complexity of triangulation ranges from $O(N)$ to $O(N^2)$, where N represents the number of grid nodes.

Some authors share their progress in adaptive grid construction through open-source contributions. For instance, Engwirda (2005, [26]; 2014, [27]) published a package that constructs an unstructured mesh for two-dimensional areas of intricate shape. This package offers high functionality for adaptive triangulating non-simply connected regions with complex boundaries.

In the context of the problem under consideration, our scope is confined to constructing a triangulation for numerically solving a system of integral equations. An initial attempt was made to employ the package mentioned above; however, it turns out that, while on the one hand, the capabilities of this package surpass the demands of our specific task, on the other

DOI: 10.37943/15AHSE8085

hand, the package does not contain functions for refining the mesh in the proximity of multiple lines, with a specified level of refinement, and for generating a triangulation on multiple intersecting surfaces. For the triangulation of contact surfaces within the examined media structure, we propose the development of a grid that has increased density at the vicinity of the measurement line and contact boundaries and adapts the positions of nodes to intersecting lines between two contact boundaries.

Mathematical model and adaptive triangulation of surfaces

1. The mathematical model formulated in terms of integral equations. Figure 1 illustrates a typical cross-section of the dam. It is important to note that this representation includes several types of contact boundaries: dam-air, dam-water, dam body-dam base, dam-leak, leak-water, leak-base, water-base, water-air, and potentially air-base. To simplify the notation, we will use the indices 0, 1, 2, 3, and 4 to represent air, dam material, water, base material, and the leaking area, respectively.

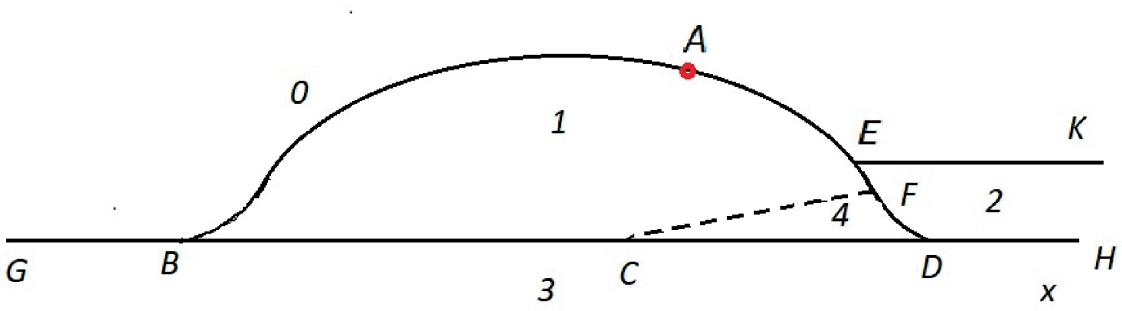

Figure 1. Schematic representation of the dam cross-section;
0 – air, 1 – dam body, 2 – water, 3 – base, 4 – possible leakage area.

Let us show briefly the main steps of deriving the mathematical model, following the monograph (Mukanova and Modin, 2018, [13]) and the article (Mirgalikyzy et al., 2015, [28]). Here, we generalize the approach for an arbitrary number of contact boundaries. The mathematical model of the ERT method is based on equations for the electric field potential U, expressed as Laplace's equation

$$\Delta U = 0 \tag{1}$$

for homogeneous media and conditions of continuity of current at contact surfaces between two media. According to Ohm's law, the current density is equal to the product of the specific conductivity and the normal derivative of the potential U:

$$I = \frac{\partial U}{\partial \mathbf{n}} \tag{2}$$

Next, we express the equality of currents passing through the surface from one side to another at any point P as follows:

Scientific Journal of Astana IT University
ISSN (P): 2707-9031 ISSN (E): 2707-904X
VOLUME 15, SEPTEMBER 2023

$$\sigma_{+}\frac{\partial U}{\partial \mathbf{n}^{+}}(P)\Big|_{\Gamma}=\sigma_{-}\frac{\partial U}{\partial \mathbf{n}^{-}}(P)\Big|_{\Gamma}, \tag{3}$$

here $\sigma_{\pm}$ are specific conductivities of the media from two sides of the boundary Γ; $\mathbf{n}$ denotes a normal vector with respect to the boundary, and the "±" signs indicate that the derivatives are taken as one approaches the boundary point P from different sides.

Let us use the double index (kl) to denote the contact boundaries between media identified by indices k and l. To satisfy equation (1) for the homogeneous part of the material, we express the function $U(P)$ at point P in terms of two components: the 'simple layer potential' of charges $q_{kl}(P)$ distributed on the contact surfaces and the standard potential arising from the pointwise source at the supply electrode A:

$$U(P)=\frac{1}{2\pi}\sum_{k,l}\iint_{\Gamma_{kl}}\frac{q_{kl}}{|\mathbf{r}_P-\mathbf{r}_Q|}d\Gamma_{kl}(Q)-\frac{1}{2\pi|AP|}\ . \tag{4}$$

We can now substitute the expression (4) into the continuity condition (3) for each boundary. Note that when point P belongs to the boundary Γ_{kl}, the normal derivatives from both sides of the boundary satisfy the following equalities (refer to, for instance, Vladimirov's textbook, 1971, [29]):

$$\begin{aligned}
&\frac{\partial}{\partial \mathbf{n}^{+}}\frac{1}{2\pi}\iint_{\Gamma_{kl}}\frac{q_{kl}(Q)d\Gamma_{kl}(Q)}{|\mathbf{r}_P-\mathbf{r}_Q|}\Bigg|_{\Gamma_{kl}}=-q_{kl}(P)+\frac{1}{2\pi}\iint_{\Gamma_{kl}}q_{kl}(Q)\frac{\partial}{\partial \mathbf{n}_P}\frac{1}{|\mathbf{r}_P-\mathbf{r}_Q|}d\Gamma_{kl}(Q)\\
&\frac{\partial}{\partial \mathbf{n}^{-}}\frac{1}{2\pi}\iint_{\Gamma_{kl}}\frac{q_{kl}(Q)d\Gamma_{kl}(Q)}{|\mathbf{r}_P-\mathbf{r}_Q|}\Bigg|_{\Gamma_{kl}}=q_{kl}(P)+\frac{1}{2\pi}\iint_{\Gamma_{kl}}q_{kl}(M)\frac{\partial}{\partial \mathbf{n}_P}\frac{1}{|\mathbf{r}_P-\mathbf{r}_Q|}d\Gamma_{kl}(Q).
\end{aligned} \tag{5}$$

Here, the vector $\mathbf{n}_P$ denotes the normal direction to the surface Γ_{kl} at point P. Suppose that the normal vector $\mathbf{n}_P$ is directed from side k to side l for the boundary Γ_{kl}. By substituting the expression (4) into condition (3) and considering the equalities (5), we obtain the following condition at Γ_{kl}:

$$\begin{aligned}
&\sigma_k\Bigg(-q_{kl}(P)+\frac{1}{2\pi}\iint_{\Gamma_{kl}}q_{kl}(Q)\frac{\partial}{\partial \mathbf{n}_P}\frac{1}{|\mathbf{r}_P-\mathbf{r}_Q|}d\Gamma_{kl}(Q)+\\
&\qquad+\frac{1}{2\pi}\sum_{(i,j)\neq(k,l)}\iint_{\Gamma_{ij}}\frac{\partial}{\partial \mathbf{n}_P}\frac{q_{ij}}{|\mathbf{r}_P-\mathbf{r}_Q|}d\Gamma_{ij}(Q)-\frac{\partial}{\partial \mathbf{n}_P}\frac{1}{2\pi|AP|}\Bigg)\\
&=\sigma_l\Bigg(q_{kl}(P)+\frac{1}{2\pi}\iint_{\Gamma_{kl}}q_{kl}(Q)\frac{\partial}{\partial \mathbf{n}_P}\frac{1}{|\mathbf{r}_P-\mathbf{r}_Q|}d\Gamma_{kl}(Q)\\
&\qquad+\frac{1}{2\pi}\sum_{(i,j)\neq(k,l)}\iint_{\Gamma_{ij}}\frac{\partial}{\partial \mathbf{n}_P}\frac{q_{ij}}{|\mathbf{r}_P-\mathbf{r}_Q|}d\Gamma_{ij}(Q)-\frac{\partial}{\partial \mathbf{n}_P}\frac{1}{2\pi|AP|}\Bigg).
\end{aligned} \tag{6}$$

After transformation, the expression (6) is reduced to the following system of integral equations:

DOI: 10.37943/15AHSE8085

$$\begin{cases} q_{kl}(P) = \dfrac{\kappa_{kl}}{2\pi} \sum\limits_{\substack{i,j \\ 1\le i<j\le 3}} \iint\limits_{\Gamma_{ij}} q_{ij}(Q) \dfrac{\partial}{\partial \mathbf{n}_P} \dfrac{1}{|\mathbf{r}_P - \mathbf{r}_Q|} d\Gamma_{ij}(Q) - \dfrac{\kappa_{kl}}{2\pi} \dfrac{\partial}{\partial \mathbf{n}_P} \dfrac{1}{|\mathbf{r}_P - \mathbf{r}_A|}, \\ (k,l) = (0,1),(0,2),(1,2),(1,3),(1,4),(2,3),(2,4),(3,4),(0,3); \quad \mathbf{r}_P = (x,y,z), \quad \mathbf{r}_Q = (x',y',z'). \end{cases} \tag{7}$$

Here, $q_{kl}(P)$ represents sought-for functions defined on the surfaces Γ_{kl}. The coefficients κ_{kl} are equal to the reflection coefficient of the contacting media along the surface Γ_{kl}: $\kappa_{kl} = (\sigma_k - \sigma_l)/(\sigma_k + \sigma_l)$.

2. Definition of areas where the finer computational grid is desirable.

To solve the system (7) numerically, we need to construct a triangulation of the contact surfaces Γ_{kl}. Most of these boundaries exhibit a 2D structure and represent the bands aligned along the direction of the dam. The cross-sections of these bands are defined by segments GB, BA, AE, BC, CD, DH, and EK in Fig.1. Computational analyses conducted by Migrgalikyzy et al. (2015, [28]) have revealed that in the vicinity of areas where the terrain transitions to a planar surface, such as points B and D, anomalous extrema in the apparent resistivity curves appear. Consequently, a dense grid near these points is deemed favorable. Moreover, the grid density must be increased along the measurement line passing through point A, as supported by simulations (Migrgalikyzy et al., 2015 [28] and Turarova et al., 2022, [10]). As shown in Figure 1, point E corresponds to the boundary between the dam, water, and air. Numerical simulations of the electrical field and apparent resistivities, as described in (Rakisheva and Mukanova, 2021, [11]) and (Rakisheva et al., 2020, [12]), illustrate significant anomalies of the electric field in the proximity of this boundary. Consequently, refining the grid near this point is desirable. Points G, K, and H are located far from source A. The electric field significantly decreases in these areas, allowing for a coarser grid. To summarize, the triangulation of bands GB and EK requires a denser grid on one side, whereas segments BA and AE necessitate a finer grid on both sides of their respective bands.

3. Construction of the grid. We construct the grid by creating non-uniform triangulations for boundaries with longitudinal structures. The sizes of the triangles are primarily determined by the *Ox* direction, and they are built layer by layer, increasing in height.

The triangle's most minor edge and the ratio between the largest and smallest edges influence the grid size. When constructing the dam's surface triangulation, we employ a curvilinear coordinate, χ, transversal to the dam's longitude, transforming the Cartesian coordinate, *x*, into curvilinear coordinates, χ. If the function $z = f(x)$ defines the shape of the contact boundary of the dam and air, then the transformation $\chi = \chi(x)$ and its inverse $x = x(\chi)$ are determined by the following ordinary differential equations:

$$\frac{d\chi}{dx} = \sqrt{z'^2(x)+1}, \quad \chi(0) = 0;$$
$$\frac{dx}{d\chi} = \frac{1}{\sqrt{z'^2(x)+1}}, \quad x(0) = 0.$$

The triangles are placed layer by layer, changing their positions along the χ coordinate. Let us define how the height $h_i = \chi_{i+1} - \chi_i$ of each layer varies in the χ direction. Suppose

$$h_\xi = \ln(1+\alpha(b-a))/N, \quad \xi_i = h_\xi \cdot i, \quad i = \overline{0,N}. \tag{8}$$

Scientific Journal of Astana IT University
ISSN (P): 2707-9031 ISSN (E): 2707-904X
VOLUME 15, SEPTEMBER 2023

Here, N is the number of points layers. Then for $a \le \chi_i \le b$ we define χ_i as follows:

$$\chi_i = a + (\exp(\xi_i) - 1)/\alpha \ . \tag{9}$$

At each layer of triangles, the ordinates of vertices are spaced at intervals of $h_{i,y} = 2(\chi_{i+1} - \chi_i)/\sqrt{3}$ along the Oy axis. This choice ensures that the triangles at each layer are 'almost' equilateral. Next, we apply the standard $delaunay(.,.)$ function from the Matlab package to two consecutive points layers to obtain their connectivity lists. These lists are then incorporated into the resulting connectivity list.

In formulas (8)-(9), the mesh condenses at the left end, $x = a$. Applying the linear transformation $-x + (a + b)$ to the interval $[a, b]$ helps achieve mesh condensation at the right end, $x = b$.

In equation (8), the parameter α controls the grid's nonuniformity. A higher α results in more significant differences in triangle sizes across layers. This parameter depends on the ratio between the sizes of the smallest and largest triangles.

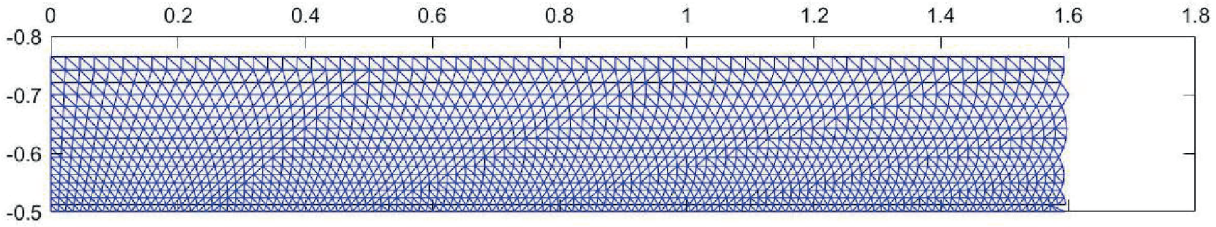

Figure 2. Typical triangulation of the left band on the surface of the base, corresponding to the cross-section GB

We require a finer grid on both edges for the bands BA and AE. In this case, the analog of formulas (8)-(9) is applied to both the left and right halves of the interval $[a, b]$.

Figure 2 shows typical examples of the triangulation for the left band GB, while Fig. 3 illustrates the densified triangulation along both edges of bands BA and AE. In this configuration, the grid is refined along the sounding line, which passes through point A, as depicted in Fig. 1, and runs parallel to the strike direction. Furthermore, grid points are concentrated at the intersections of the contact surfaces.

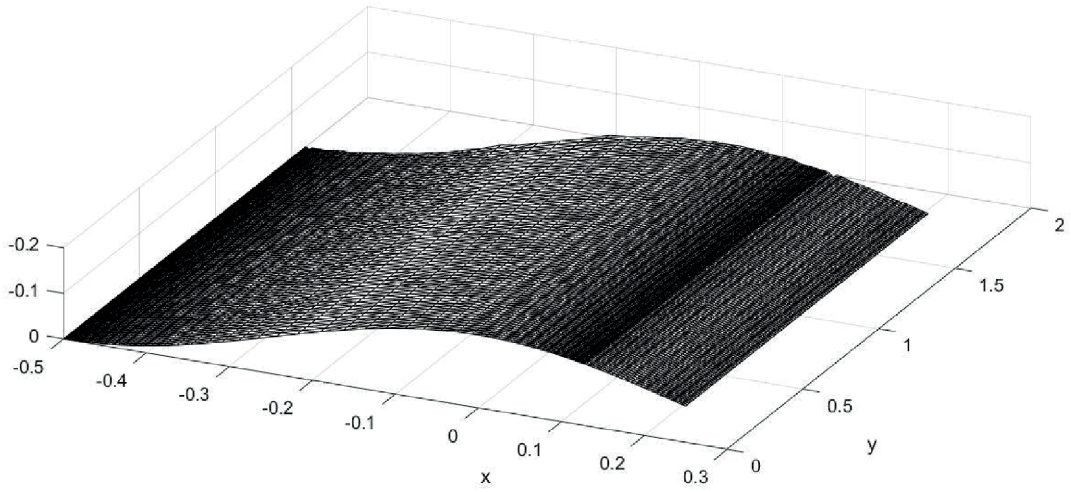

Figure 3. Triangulation of the bands on the dam's surface condensed at the bands' edges.

DOI: 10.37943/15AHSE8085

Now, we need to construct the grid for surfaces that represent the boundaries of the leaking area. The leakage is bounded along the longitude axis Oy, so the triangulation of the boundaries leakage-base, leakage-dam, leakage-water, and part of the dam placed on the band with the cross-section CD must be built separately.

Figure 4 shows one example of the possible triangulation of the considered dam model.

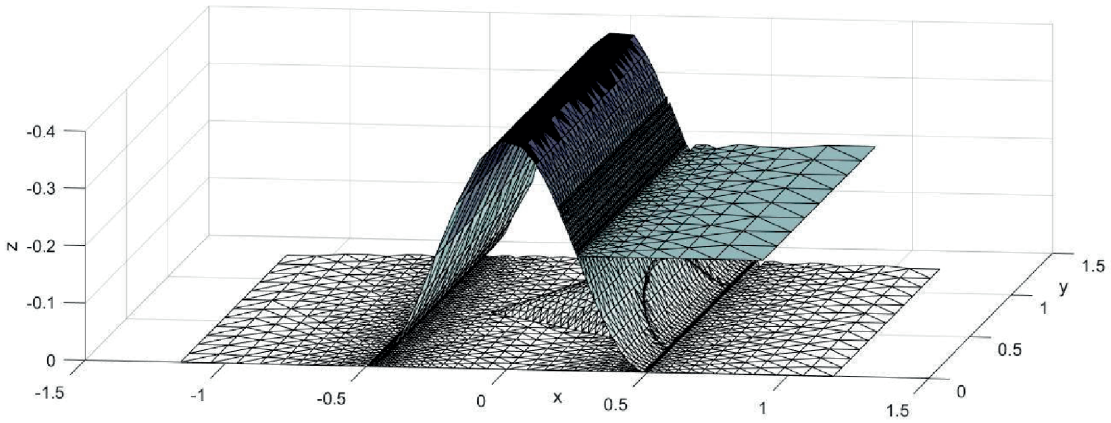

Figure 4. Triangulation of the computing area by adapting the mesh to the geometric and electrical features of the media.

First, the triangulation of the bands along the Oy axis, defined by their cross-sections BD and ED, is generated using the abovementioned method. Subsequently, we identify the boundary points for the contacts leaking area – dam and base – leakage. These points are then incorporated into the band ED and BD triangulation using the Matlab function *delaunay*(.,.), as illustrated in Fig. 5.

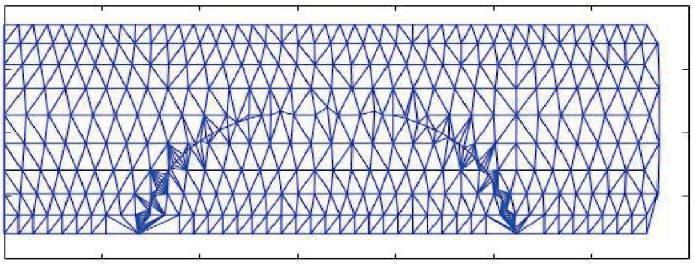

Figure 5. Fragment of the triangulation of the boundaries Leakage- water and dam-water

To model the form of the leaking area, we have chosen the conic surface defined by the following formula:

$$(y-y_0)^2 / c^2 + z^2 <= r^2 (x-x_0)^2 . \quad (10)$$

Here, the parameters (x_0, y_0) define the position of point C, and the parameters c and r define the geometrical properties of the leaking area. This formula makes it possible to build the triangulation again layer by layer in the direction of the Ox axis. Figure 4 shows one example of the possible triangulation built for the described case of the media. An example of the triangulation of the leaking area is shown in Fig. 6 separately.

Scientific Journal of Astana IT University
ISSN (P): 2707-9031 ISSN (E): 2707-904X
VOLUME 15, SEPTEMBER 2023

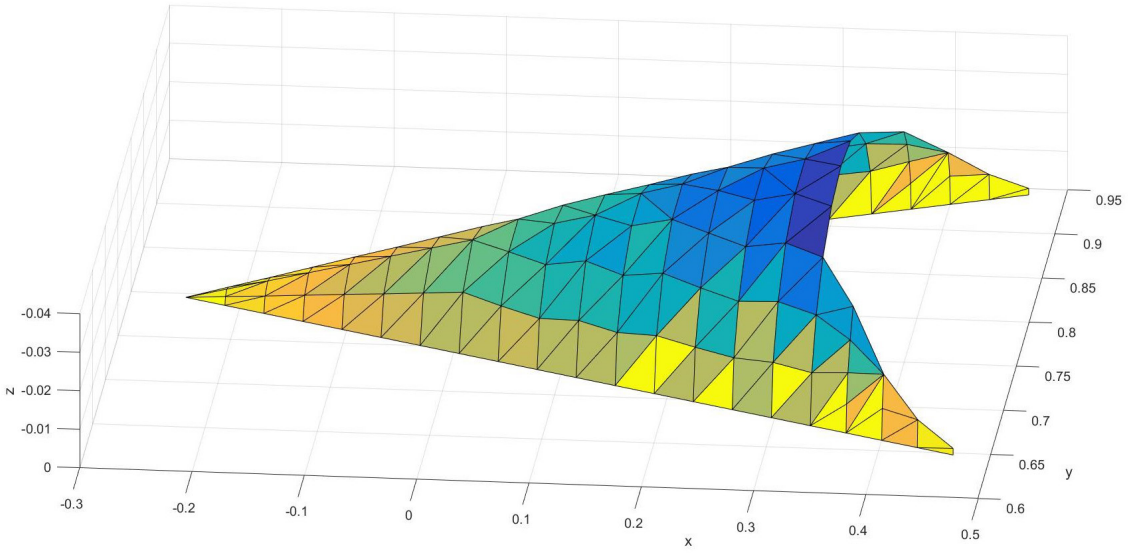

Figure 6. The triangulation of the boundary dam-leaking area

As it is previously mentioned, the triangulations were constructed layer by layer. We determined the layer's thickness along the Ox axis and the positions of points along the Oy direction for each layer. Then, we have applied the Matlab function $delaunay(.,.)$ for two subsequent rows of points. The corresponding number of vertexes is then added to the triangulation connectivity list and the list of nodes.

Finally, we compared the number of nodes for homogeneous and adaptive grids, using equal values for the minimal grid step and considering a non-uniformity parameter $\alpha = 5$ as defined in (8), with the dam's geometry shown in Fig. 4. We found that the number of nodes is $N_{\text{un}} = 11368$ for the uniform grid and $N_{ad} = 4\,153$ for the non-uniform grid. This allows us to estimate that the size of the dense matrix in the discretization of the system of equations (7) is approximately $N_{un}^2 / N_{ad}^2 \approx 7.5$ times smaller for the adaptive grid.

Conclusion

In this study, we have formulated an ERT mathematical model applicable to media characterized by piecewise distributed conductivity functions and an arbitrary number of contact boundaries. The methodology described here focuses on constructing an adaptive grid by triangulating contact boundaries within 3D space to solve the associated system of integral equations. The grid is adapted to the specific characteristics of the media, particularly in the context of a dam with a leakage area.

Curvilinear coordinates are employed, facilitating the construction of an appropriate grid on the dam's surface. The selection of regions for grid refinement is determined by considering the outcomes of prior mathematical modeling of the ERT method for relief surfaces. The direction across the dam body has been selected to enhance grid refinement. Subsequently, the delaunay(.,.) function is applied layer-by-layer.

In the case of a cross-section involving two contact surfaces, crossline points are explicitly defined and incorporated into the pre-existing nodes, resulting in the generation of a new triangulation. This approach effectively constructs an adaptive triangulation that explicitly encompasses the cross-lines of surfaces within the triangulation structure.

Comparing the node counts between homogeneous and non-homogeneous grids reveals a significant reduction in the matrix size for the discretized version of the integral equa-

tions, signifying the computational advantages of our approach. Future research endeavors will center on solving the system of integral equations (7) under varying physical conditions and optimizing the grid's computational parameters for increased simulation efficiency and accuracy. If the proposed method is effectively executed, it has the potential to complement the hydraulic structures databases with real-time mathematical modeling capabilities.

Acknowledgment

The author expresses her deep gratitude to the anonymous referees whose comments helped significantly improve the presentation of the results.

This research is funded by the Science Committee of the Ministry of Science and Higher Education of the Republic of Kazakhstan (Grant No. AP14869144 "Development of systematic geophysical monitoring for the safe operation of water management facilities").

References

[1] Barker, R.D. (1981). The offset system of electrical resistivity sounding and its use with a multicore cable. *Geophysical Prospecting,* 29(1), 128-143.

[2] Barker, R.D. (1993). A simple algorithm for electrical imaging of the subsurface. *First Break*, 10(2), 53-62.

[3] Dahlin, T. (1993). *On the automation of 2D resistivity surveying for engineering and environmental applications* [PhD thesis]. Lund University.

[4] Dahlin, T. (1996). 2D resistivity surveying for environmental and engineering applications. *First Break*, 14, 275–283.

[5] Dahlin, T. (2001). The development of DC resistivity imaging techniques. *Computers &Geosciences,* 27, 1019–1029.

[6] Dahlin, T. & B. Zhou, B. (2004). A numerical comparison of 2D resistivity imaging with 10 electrode arrays. *Geophysical Prospecting*, 52, 379-398.

[7] Gunther, T. & Rucker, C. (2013). Boundless Electrical Resistivity Tomography. *BERT 2 - the user tutorial,* Ver.2.0.

[8] Loke, M.H. & Barker, R.D. (1996). Rapid least-squares inversion of apparent resistivity pseudosections using a quasi-Newton method. *Geophysical Prospecting*, 44, 131-152.

[9] Loke, M.H. (2000). Topographic modeling in electrical imaging inversion. *62nd Conference and Technical Exhibition*, EAGE, Extended Abstracts, D-2.

[10] Turarova, M., Mirgalikyzy, T., Mukanova, B., Modin, I., & Kaznacheev, P. (2022). Evaluation of the 3D Topographic Effect of Homogeneous and Inhomogeneous Media on the Results of 2D Inversion of Electrical Resistivity Tomography Data. *Modelling and Simulation in Engineering*. https://doi.org/10.1155/2022/5196686

[11] Rakisheva, D., & Mukanova, B. (2021). Fourier Transformation method for solving integral equation in the 2.5 D problem of electric sounding. *Journal of Physics: Conference Series*, 2092(1), 012018. https://iopscience.iop.org/article/10.1088/1742-6596/2092/1/012018/pdf.

[12] Rakisheva, D., Mukanova, B., & Modin, I. (2020). Simulation Of Electrical Monitoring Of Dams With Leakage With A Transverse Placement Of The Measuring Installation. *Eurasian Journal of Math. and Computer Appl.*, 8(4), 69-82. https://doi.org/10.32523/2306-6172-2020-8-4-69-82

[13] Mukanova, B., & Modin, I. (2018). The Boundary Element Method in Geophysical Survey. *Springer.* ISBN 978-3-319-72908-4. https://link.springer.com/book/10.1007/978-3-319-72908-

[14] Shi-zhe, Xu. (2001). The Boundary Element Method in Geophysics. *Geophysical Monograph Series*, (9), SEG Books, 217.

[15] Zhdanov, M., & Michael, S. (2015). Geophysical Inverse Theory and Applications. *Elsevier,* 2,730.

[16] Turarova, M., Mirgalikyzy, T., Mukanova, B., & Modin, I. (2022). Elimination of the ground surface topographic effect in the 2d inversion results of electrical resistivity tomography data. *Eurasian Journal of Math. and Computer Appl.*, 10(3), 84–104.

Scientific Journal of Astana IT University
ISSN (P): 2707-9031 ISSN (E): 2707-904X
VOLUME 15, SEPTEMBER 2023

[17] Frey, P.J. & George, P. (2008). Mesh Generation: Application to Finite Elements. *ISTE Ltd,* https://doi.org/10.1002/9780470611166
[18] Cuillière, JC. (1998). An adaptive method for the automatic triangulation of 3D parametric surfaces. *Computer-Aided Design*, 30(2), 139–149. https://doi.org/10.1016/s0010-4485(97)00085-7
[19] Lo, S. H. (2002). Finite element mesh generation and adaptive meshing. *Progress in Structural Engineering and Materials*, 4(4), 381–399. https://doi.org/10.1002/pse.135
[20] Feng, L., Alliez, P., Busé, L., Delingette, H., & Desbrun, M. (2018). Curved optimal delaunay triangulation. *ACM Transactions on Graphics*, 37(4), 1-16. https://doi.org/10.1145/3197517.3201358
[21] Schmidt, P.P., & Kobbelt, L. (2023). Surface Maps via Adaptive Triangulations. *Computer Graphics Forum*, 42(2), 103 – 117. https://doi.org/10.1111/cgf.14747
[22] Shewchuk, J. R. (2000). Delaunay refinement algorithms for triangular mesh generation. *Computational Geometry: Theory and Applications*, 22, (1-3), 21–74. https://doi.org/10.1016/S0925-7721(01)00047-5
[23] Meng, X., & Mei, G. (2013). Robust delaunay triangulation for domain with acute angles. *Proceedings of SPIE - The International Society for Optical Engineering*, 88782013(88783D) 5th International Conference on Digital Image Processing, ICDIP 2013. https://doi.org/10.1117/12.2031767
[24] Schier, A., & Klein, R. (2023). Discrete exterior calculus for meshes with concyclic polygons. *Computer Aided Geometric Design*, 101(C), 102170. https://doi.org/10.1016/j.cagd.2023.102170
[25] Shewchuk, J.R. (2012). *Lecture Notes on Delaunay Mesh Generation*. University of California at Berkeley, Berkeley. delnotes.dvi (berkeley.edu)
[26] Engwirda, D. (2014). *Locally-optimal Delaunay-refinement and optimisation-based mesh generation* [Ph.D. Thesis, School of Mathematics and Statistics]. The University of Sydney.
[27] Engwirda, D. (2005). *Unstructured mesh methods for the Navier-Stokes equations*. [Honours Thesis, School of Aerospace, Mechanical and Mechatronic Engineering]. The University of Sydney.
[28] Mirgalikyzy, T., Mukanova, B., & Modin, I. (2015). Method of Integral Equations for the Problem of Electrical Tomography in a Medium with Ground Surface Relief. *Journal of Applied Mathematics*. DOI: http://dx.doi.org/10.1155/2015/207021.
[29] George, B.A., Hans, J.W., & Frank, E.H. (2012). Mathematical Methods for Physicists. *Elsevier,* 7. DOI: https://doi.org/10.1016/C2009-0-30629-7